Evolution and nucleosynthesis in low mass Asymptotic Giant Branch stars

S. Cristallo([1])

([1]) *Osservatorio Astronomico di Teramo (INAF) - via Maggini, 64100, Teramo (Italy)*

Summary. — People usually smile when astrophysicists assert that we are *sons of the stars*, but human life confirms this sentence: about 65% of the mass of our body is made up of oxygen, carbon occurs in all organic life and is the basis of organic chemistry, nitrogen is an essential part of amino acids and nucleic acids, calcium is a major component of our bones. Moreover, phosphorus plays a major role in biological molecules such as DNA and RNA (where the chemical codes of life is written) and our blood carries oxygen to tissues by means of the hemoglobin (an iron pigment of red blood cells). All these elements have been created in stars. I just list some examples related to human body, but also common element such as aluminum, nickel, gold, silver and lead come from a pristine generation of stars. The abundances in the Solar System are in fact due to the mixing of material ejected from stars that polluted the Universe in different epochs before the Sun formation, occurred about 5 billion years ago, after the gravitational contraction of the proto-solar cloud. Low mass AGB stars ($1<M/M_{\odot}<3$) are among the most important polluters of the Milky Way, because of the strong winds eroding their chemically enriched envelopes. They are responsible for the nucleosynthesis of the main component of the cosmic s-elements.

PACS 97.10.Cv – Stellar structure, interiors, evolution, nucleosynthesis, ages.
PACS 97.10.Tk – Abundances, chemical composition.

1. – Introduction

The majority of the isotopes heavier than iron (A≥56) are synthesized by neutron capture processes. The observed heavy elements distribution shows the presence of two main components, correlated to different nucleosynthetic processes: the s (slow) process and the r (rapid) process (on the basis of the definitions given by [1] in their pioneering work). The r process requires high neutron densities, and it is believed to occur during explosive phases of stellar evolution (Novae, SuperNovae and/or X-rays binaries). The s process is characterized by a slow neutron capture with respect to the corresponding β decay: stable isotopes capture neutrons, while the radioactive ones decay (β^- or β^+) or capture a free electron. These isotopes are mainly created in the Thermally Pulsing AGB (TP-AGB) phase of low mass stars ($1 \leq M/M_{\odot} < 4$), where freshly synthesized elements

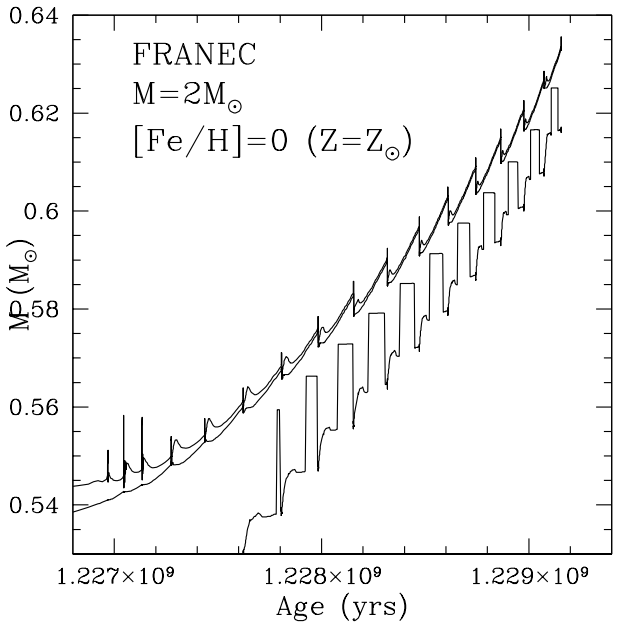

Fig. 1. – Evolution of the positions in mass of the inner border of (top to bottom): convective envelope, H-burning shell and most energetic mesh of the He-burning shell, during the Thermally Pulsing AGB phase of a model with initial mass M=2M$_\odot$ and solar metallicity..

are carried out to the surface by means of a recurrent mechanism called Third Dredge Up (TDU) (see [2] and references therein). In this phase the stellar structure consists of a partially degenerate carbon-oxygen core, an He shell separated from an H shell by the He-intershell region and by a convective envelope (see Fig.1). The energy required to supply the surface irradiation is mainly provided by the H burning shell, located just below the inner border of the convective envelope. This situation is recurrently interrupted by the growing up of thermonuclear runaways, driven by violent He-burning ignitions. As a consequence of a Thermal Pulse (TP), the region between the two shells (He-intershell) becomes unstable against convection (for a short period), the external layers expand and, later on, the H shell burning temporarily dies down. In the He-intershell, He is partially converted into carbon. During the AGB phase, main neutron sources are the ^{13}C(α,n)^{16}O reaction, active in radiative layers during the interpulse period [4], and the ^{22}Ne(α,n)^{25}Mg reaction, marginally activated within the convective shell originated by the TP. In order to obtain a sufficient amount of ^{13}C for the activation of the s-process, a diffusion of protons from the H-rich envelope into the ^{12}C-rich radiative zone is needed: the diffused proton are captured from the abundant carbon via the ^{12}C(p,γ)^{13}N(β^-)^{13}C nuclear chain, leading to the formation of a tiny ^{13}C-pocket.

2. – The ^{13}C pocket and the nuclear network

A major improvement in our stellar evolution code is the introduction of a physical algorithm for the treatment of the convective/radiative interface at the inner border of the convective envelope [3, 2]. During TDU episodes, the opacity of the envelope (H-rich) is

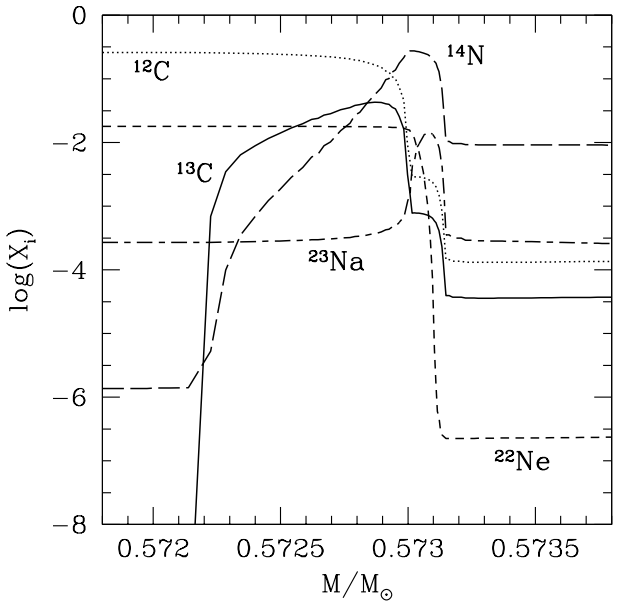

Fig. 2. – Abundances profiles in the ^{13}C pocket formed after the 3^{th} TDU episode ($M = 2M_{\odot}$ model with solar metallicity).

significantly larger than the opacity of the underlying H-exhausted (and He-rich) region. This fact causes an abrupt change of the temperature gradient at the inner border of the penetrating convective envelope. In this condition, the convective boundary becomes unstable, because any perturbation causing an excess of mixing immediately leads to an increase of the opacity and, in turn, to an increase of the temperature gradient. However, the steep pressure gradient that develops immediately below the formal border of the convective envelope limits the penetration of the instability, so that the average convective velocity should rapidly drop to zero. In order to mimic this behavior, we assume that in the region underlying the formal convective boundary, the average velocity follows an exponential decline, namely

$$v = v_{bce} \exp\left(-\frac{d}{\beta H_P}\right), \tag{1}$$

where d is the distance from the formal convective boundary, v_{bce} is the velocity of the most internal convective mesh, H_P is the pressure scale height at the formal border of the convective envelope (defined by the Schwarzschild criterion) and β is a free parameter. The partial diffusion of protons in the top layers of the He shell gives naturally rise to the subsequent formation of a ^{13}C-rich tiny layer, the so-called ^{13}C pocket. In Fig. 2 we plot the chemical profiles of trace isotopes in the region around the ^{13}C pocket. The ^{13}C pocket (solid line) partially overlaps with a more external ^{14}N pocket (long-dashed line). The maximum of the ^{14}N coincides with the region where the protons diffused from the convective envelope at the epoch of the TDU were abundant enough to allow a full CN

cycle. This is also the region where the ^{23}Na (short-dashed-long-dashed line) has been efficiently produced by the ^{22}Ne(p,γ)^{23}Na reaction. Indeed, at the end of the previous TP, the mass fraction of ^{22}Ne (short-dashed line) in the top layer of the He-rich intershell is of the order of 2×10^{-2} and, around the ^{14}N maximum, this ^{22}Ne is almost completely converted into ^{23}Na, leading to the formation of a tiny ^{23}Na pocket.

The introduction of the exponentially decaying profile of convective velocities automatically implies an assumption on the value of the free parameter β: in the models presented in this work, we assume a value β=0.1. In order to justify such a choice we perform some tests on a star with initial mass $M = 2M_{\odot}$ and different metallicities (Z=Z$_{\odot}$ and Z=1.0 $\times$ 10^{-4}). We calculate the same sequences TP-Interpulse-TP, starting from the first TP followed by TDU, and we evaluate the consequences of changing this parameter in the range $0< \beta <0.2$ (Cristallo et al., *in preparation*). While the amount of material interested by a single TDU episode increases by more than a factor of 3 from the case with no velocity profile (β=0) and the extreme case (β=0.2), the $^{13}C_{eff}$, available for the heavy elements nucleosynthesis, grows up with increasing β, reaches a maximum in correspondence of β=0.1 and then decreases down to negative values. We stress the fact that the net ^{13}C that contributes to the s-process nucleosynthesis is represented by $^{13}C_{eff}$, defined as the difference between the ^{13}C and the ^{14}N mass fractions (^{14}N is in fact a strong neutron poison via the ^{14}N(n,p)^{14}C reaction). Our result derives from a combination of two different physical processes: the growing of the $^{13}C_{eff}$ is a direct consequence of the greater efficiency of the velocity profile algorithm, while its decreasing for large β values is due to the fact that the convection efficiency in the zone interested by the velocity profile starts to be too high. This leads the most external layers of the He-intershell to be fully mixed and to consequently show an envelope-like H abundance, instead of the H profile needed for the formation of the ^{13}C pocket. We therefore propose an efficient way to calibrate the free parameter affecting the velocity profile algorithm, confining its possible values in a narrow range, and we adjust it in order to obtain the maximum ^{13}C pocket expected for the s-process nucleosynthesis.

The simultaneous solution of the stellar structure equations and a full network including all the relevant isotopes up to the termination point of the s-process path (Pb-Bi) requires a relevant computational power. For this reason, a post-process nucleosynthesis calculation, based on AGB stellar models computed with a restricted nuclear network, was generally preferred [5]. The coupling of a stellar code with a complete nuclear network has not been feasible so far, but this limitation has been overcome thanks to last generation of computers and to the adoption of smart algorithms to invert sparse matrixes of huge size. AGB models presented in this work are therefore calculated by using an extended set of nuclear processes including all chemical species involved in the s-process nucleosynthesis [6]. The models presented here have been obtained by including into the FRANEC stellar evolution code [7, 2] a full nuclear network, containing about 500 isotopes (from H to the Pb-Bi-Po ending point) linked by more than 750 reactions. Reaction rates of isotopes involving charged particles are generally taken from the NACRE compilation [8], while the neutron captures cross sections are mainly taken from [9]. Weak-interaction rates (electron captures, and β decays) are interpolated as a function of the temperature and electron density, while at temperatures lower than 10^6 K we assume a constant value equal to the terrestrial one. The presence of isomeric states of unthermalized isotopes, which lead to ramifications of the s-process flux, is followed in detail. This network is continuously upgraded according to the latest theoretical and experimental nuclear physics improvements.

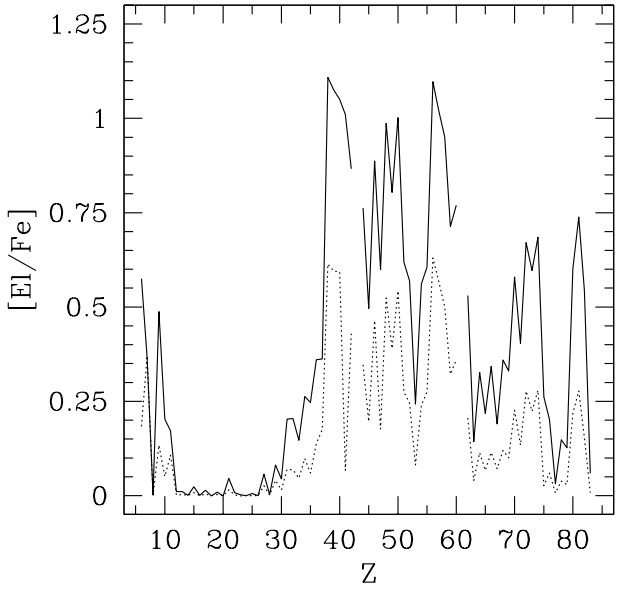

Fig. 3. – Surface composition of a model with M=2M$_\odot$ and solar metallicity after the fifth TDU (dotted curve) and the last TDU (solid curve).

3. – Low temperature C-enhanced opacities

The FRANEC models benefit of another important improvement, whose effects are particularly important at low metallicities: the introduction of C-enhanced low temperature opacities. In principle, a stellar evolutionary code should account for the variations of the envelope chemical composition; in practice, only variations of the main constituents (H and He) are usually considered. Nevertheless, in the atmosphere of an AGB star, both C dredge-up and the possible conversion of C into N (by CN cycle) substantially affect the molecular contribution to the opacity for temperatures lower than 4000 K. This is due to the fact that, when a carbon excess is present (i.e. when the number ratio C/O>1), carbon bearing molecules (C_2, CN, C_2H_2, C_3) start forming and their contribute to opacity become dominant. Therefore, in order to overcome this limitation, we calculate low temperature C- and N-enhanced opacity tables, suitable for AGB model calculations [10]. The new AGB models succeed in reproducing the photometric and spectroscopic properties of their observational counterparts (see Section **6**).

4. – Solar metallicity model

The final C/O envelope ratio in the solar metallicity model is 1.88, while it becomes larger than 1 when the core mass is about 0.6 $M_\odot$ and the bolometric magnitude is about -5.0 mag, in good agreement with the Galactic C-star luminosity function [11]. A ^{13}C pocket, whose mass extension decreases pulse after pulse, forms after each TDU episode. The ^{13}C in the first pocket is only partially burnt during the interpulse and

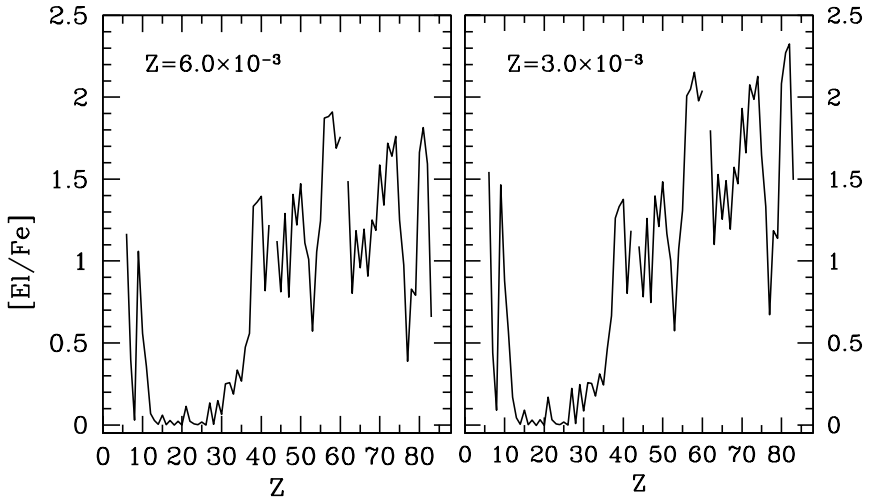

Fig. 4. – Surface compositions of models with M=2M$_\odot$ and Z=6.0 $\times$ 10^{-3} (left Panel) and Z=3.0 $\times$ 10^{-3} (right Panel).

the residual is engulfed into the convective zone generated by the subsequent TP. In this case, the ^{13}C burning takes place at the bottom of the convective shell ($T \sim 1.6 \times 10^8$ K) producing a very high neutron density, this fact implying interesting peculiarities on the following nucleosynthesis (see [12]). In particular, some branchings, which remain closed during a standard radiative ^{13}C burning and are marginally activated during the ^{22}Ne(α,n)^{25}Mg burning, are now open: in a very short temporal step ($\Delta T < 3$ years) we obtain a consistent production of neutron-rich isotopes normally by-passed by the standard radiative ^{13}C s-process, among which ^{60}Fe, ^{86}Kr, ^{87}Rb and ^{96}Zr. Concerning the standard radiative s-process nucleosynthesis, all the elements (from Sr to Pb) result enhanced. We find that the abundance of Sr, Y and Zr at the first s peak, the so-called ls elements (*light* s elements), is comparable with the one of the hs elements (*heavy* s elements) Ba, La, Ce, Pr, Nd at the second s peak (see Fig. 3). Lead is under-produced with respect barium. The [hs/ls] ([1]) attained in the envelope when C/O=1 is in good agreement with those measured in galactic C(N) giants [13].

5. – Intermediate metallicity models

The ^{13}C(α,n)^{16}O reaction (the main source of neutrons) is primary-like, i.e. not directly affected by the metallicity of the pristine material. However, since the build-up of heavy nuclei requires neutron captures starting from Fe seeds, the s-process is expected to decline with metallicity (it is therefore of secondary nature). Nevertheless, while the iron seeds scale with the metallicity, when decreasing the number of iron seeds the number of neutrons available per seed is larger. The dependence of s-process yields at different

([1]) We use the standard spectroscopic notation [A/B]=log(N(A)/N(B))$-$log(N(A)/N(B))$_\odot$.

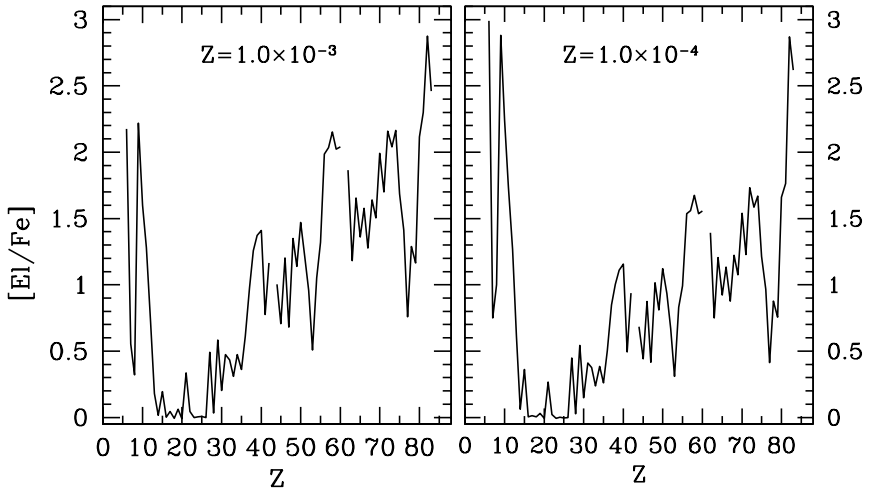

Fig. 5. – Surface compositions of models with M=2M$_\odot$ and Z=1.0 $\times$ 10^{-3} (left Panel) and Z=1.0 $\times$ 10^{-4} (right Panel).

metallicities is therefore very complex and non linear (see e.g. [14]). At metallicities Z$\sim$ (3 $\div$ 6) $\times$ 10^{-3} the s-process distribution is peaked around the hs elements (see Fig. 4). Moreover, we obtain an increase in the relative production of carbon and fluorine with decreasing the metallicity: this is a direct consequences of the greater efficiency of the TDU episodes, when the convective envelope penetrates into the ^{12}C-rich He-intershell (see [15]). We want to stress the fact that the production of ^{12}C is of primary nature (it is in fact produced by the activation of the triple α reaction in the He-intershell). The nature of the fluorine production, that basically depends on the nucleosynthesis of ^{15}N (see e.g. [16]) is more complex, being partly of primary nature (due to the contribution of the ^{13}C pocket) and partly of secondary nature (due to the contribution of the ashes of the H-burning shell). Finally, let us note that at these metallicities the production of lead (mainly ^{208}Pb) starts being very efficient.

6. – Low metallicity models

At low metallicities, most of the seeds are converted into ^{208}Pb, at the termination point of the s-process fluency (see e.g. [17]). Trends illustrated in Fig. 5 (which relates to the $Z = 1\times10^{-3}$ and to the $Z = 1\times10^{-4}$ models) confirm the previous sentence: a consistent lead production (Z=82) is in fact found in both models. As already stressed in the previous Section, the lower the metallicity is, the larger surface carbon overabundances are found: [C/Fe]$\sim$2.2 at Z=1×10^{-3} and [C/Fe]$\sim$3.0 at Z=1×10^{-4}.
Low metallicity stars enriched in s-process elements show consistent enhancements in the hs region, spanning in the range 0.8<[hs/Fe]<2.3 . Even if our final [hs/Fe] value lays within the observed range, we cannot reproduce the observed spread with a single evolutionary model. In spite of this, we want to point out the importance of the opacity coefficients on the stellar evolution of low metallicity models. As already outlined

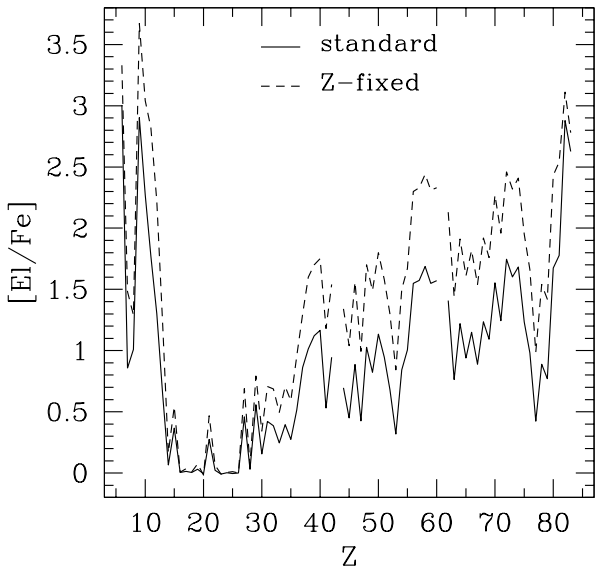

Fig. 6. – Surface compositions of a model with M=2M$_\odot$ and Z=1.0×10^{-4}. The solid line refers to our *standard* model; the dashed line refers to a model with the same initial inputs but with a different opacity treatment (*Z-fixed* model). See text for details.

in Section **3**, in our models the opacity change caused by the variation of the internal chemical composition has been taken into account by linearly interpolating between tables with different carbon, nitrogen and helium abudances [10]. However, the procedure followed by the majority of modelers is to adopt the opacity coefficients calculated at the initial metallicity and to use them for the entire evolution. In order to evaluate the possible effects induced by these different opacity treatments, we compute another model at Z=1×10^{-4} by using for the entire evolution the opacity coefficients calculated for the initial metallicity (we refer to this calculation as the *Z-fixed* case) and we compare it with respect to the Z=1×10^{-4} model already presented (*standard* case). The TP-AGB phase of the *Z-fixed* case is longer (a factor of 2 more than the *standard* model), this implying a natural increase in the number of TPs followed by TDU (N=49 with respect to the 15 found in the *standard* model). Consequently, the surface abundances of the *Z-fixed* case are larger with respect to the *standard* case (see Fig. 6), showing a better agreement with observations. We argue that these difference in the surface distributions are due to the mass loss rate, which results less efficient in the *Z-fixed* model with respect to the *standard* case, due to the fact that the surface temperature is always larger and the radius is less expanded [18]. As a consequence of so different mass-loss rate histories, in the *Z-fixed* case we find a large increase of the total dredged up material during the AGB phase with respect to the *standard* case and, therefore, the resulting final heavy element enhancements result larger. Our results seem therefore to suggest that the model computed with opacity tables at fixed metallicity is more efficient in reproducing spectroscopic data. There are however observational counterparts supporting the opposite

conclusion, driven by the study of C-stars in Dwarf Spheroidal Galaxies (DSGs); we refer in particular to the Draco Dwarf Spheroidal Galaxy [19, 20]. The observed giants belonging to this DSph present surface temperatures in the range 3.55<logT<3.61 . Note that this range is never attained by the *Z-fixed* case, while it is entirely spanned by the *standard* case (see Fig.4 in [10]).
Another important aspect which has to be addressed is the choice of the mass-loss history. Actually, observation cannot lead modelers in parameterizing the mass-loss at low metallicities, basically due to the fact that up to date a clear determination of the gas-to-dust ratio (needed to properly calculate the mass-loss) has not been feasible at non-solar metallicities [21, 22]. For this reason we adopt the same mass-loss history at all metallicities (see [2] for a description of our choice). Preliminary results show however that when using a different (milder) mass-loss [23] the surface overabundances increase on average for 0.2 deX (Cristallo et al. *in preparation*).
Another source of uncertainty in modelling AGB stars at low metallicity is the choice of the mixing length parameter, which has been calibrated by calculating a Standard Solar Model. If using initial abundances from [24], we fit the observed properties of the Sun by using a value of the mixing length parameter $\alpha_{m.l.}$=2.1 (see [25]). Due to the current lack of indications for the assumption of a different $\alpha_{m.l.}$ value at low metallicities, we adopt the same value at all metallicities: preliminary results indicate however that when using a lower value (i.e. $\alpha_{m.l.}$=1.8) the surface overabundances decrease on average for 0.2 deX (Cristallo et al, *in preparation*).

7. – Very low metallicity models

In the case of very metal poor AGBs, we find that, for a given metallicity, there exists a lower mass limit for which normal AGB evolution may occur [10]. Stars with smaller initial mass experience protons engulfment episodes during the first fully developed TP (see e.g. [26, 27]), which lead to a peculiar s-process nucleosynthesis, a low $^{12}C/^{13}C$ and a significant synthesis of primary N. Owing to the low entropy barrier, protons are engulfed within the He-intershell, where the high temperature and the large C abundance induce a violent H-burning flash. The consequent synthesis of ^{13}C allows the activation of the $^{13}C(\alpha,n)^{16}O$ reactions and a very large neutron density is attained. Thus, the production of neutron-rich nuclei, normally by-passed by a standard s-process, can occur in these stars. Later on, when the intershell cools down, a deep TDU occurs. Since in the envelope the C/O becomes grater than 1, the large N abundance favors the formation of CN molecules, thus inducing a further increase of the radiative opacities. This new set of very low metallicity models, that represents the current frontier of AGB modelling, is still under analysis.

8. – Conclusions

The present work demonstrates that, nowadays, the computational power allows the coupling between a stellar evolutionary code and a full nuclear network. A different treatment of the internal border of the convective envelope with respect to a bare Schwarzschild criterion allows the formation of the so-called ^{13}C pocket. For the first time in the literature, it has been possible to directly compare theoretical models and observational data both from a physical (luminosities, surface temperatures) and a chemical (light elements and heavy elements abundances) point of view . Moreover, we furnish a uniform set of yields (from hydrogen to lead) at different metallicities. The

importance of the adopted mass loss rate and of molecules contribution to opacity has been pointed out. While the first problem is still under analysis, the second one has been solved by using opacity tables with enhanced carbon and nitrogen abundances. Finally, we have addressed the importance of very low metallicity AGB models, by describing first preliminary (and promising) results.

* * *

I sincerely thanks Prof. O. Straniero and Prof. R. Gallino for their invaluable expertise and their deep knowledge of the arguments treated in this paper. Without a continuous interaction and ideas sharing with them I would not acquire the needed scientific uprightness to make research in a proper way.

REFERENCES

[1] Burbidge, E.M., Burbidge, G.R., Fowler, W.A., Hoyle, F., *RvMP*, **29** (1957) 547.
[2] Straniero O., Gallino R. and Cristallo S., *Nucl. Phys. A*, **777** (2006) 311.
[3] Cristallo S., Straniero O., and Gallino R., *Mem. S.A.It.*, **75** (2004) 665.
[4] Straniero, O., Gallino, R., Busso, M., Chieffi, A., Limongi, M., Salaris. M., *ApJL*, **440** (1995) 85.
[5] Gallino, R., Arlandini, C., Busso, M., Lugaro, M., Travaglio, C., Straniero, O., Chieffi, A., Limongi, M., *ApJ*, **497** (1998) 388.
[6] Cristallo S., Straniero O., Gallino R., Herwig, F., Chieffi, A., Limongi, M., Busso, M., *Nucl. Phys. A*, **688** (2001) 217.
[7] Chieffi, A., Limongi, M. and Straniero, O., *ApJ*, **502** (1998) 737.
[8] Angulo, C. and 27 coauthors, *Nucl. Phys. A*, **656** (1999) 3.
[9] Bao, Z.Y. and Käppeler, F., *Atom. Data Nucl. Data Tables*, **76** (2000) 70.
[10] Cristallo, S., Straniero, O., Lederer M.T., Aringer, B., *ApJ*, **667** (2007) 489.
[11] Guandalini, R., Busso, M., Ciprini, S., Silvestro, G., Persi, P., *A&A*, **445** (2006) 1069.
[12] Cristallo, S., Gallino, R., Straniero, O., Piersanti, L., Domínguez, I., *Mem. S.A.It.*, **77** (2006) 774.
[13] Abia C. and 8 coauthors, *ApJ*, **579** (2002) 817.
[14] Travaglio, C., Galli, D., Gallino, R., Busso, M., Ferrini, F., Straniero, O., *ApJ*, **521** (1999) 691.
[15] Straniero O., Domínguez, I., Cristallo S., Gallino R., *Publ. Astron. Soc. Aust.*, **20** (2003) 389.
[16] Lugaro, M., Ugalde, C., Karakas, A., Görres, J., Wiescher, M., Lattanzio, J.C., Cannon, R.C., *ApJL*, **615** (2004) 934.
[17] Delaude, D., Gallino, R., Cristallo, S., Straniero, O., *ESO Astrophysics Symposia*, Springer-Verlag 2006.
[18] Cristallo, S., *PASP*, **118** (2006) 1360.
[19] Aaronson, M. and Mould, J., *ApJ*, **290** (1985) 191.
[20] Domínguez, I., Abia, C., Straniero, O., Cristallo, S., Pavlenko, Ya.V., *A&A*, **422** (2004) 1045.
[21] Lagadec, E., Zijlstra, A.A., Matsuura, M., Menzies, J.W., van Loon, J.Th., Whitelock, P.A., *MNRAS*, **tmp** (2007) 1089.
[22] Matsuura, M. and 13 coauthors, *MNRAS*, **382** (2007) 1889.
[23] Reimers, D., *Mem. Soc. R. Sci. Liege, 6^e Ser.*, **8** (1975) 369.
[24] Lodders, K., *ApJL*, **591** (2003) 1220.
[25] Piersanti, L., Straniero, O. and Cristallo, S., *A&A*, **462** (2007) 1051.
[26] Hollowell, D., Iben, I.Jr. and Fujimoto, M.Y., *ApJ*, **351** (1990) 245.
[27] Iwamoto, N., Kajino, T., Mathews, G.J., Fujimoto, M.Y., Aoki, W., *ApJ*, **602** (2004) 377.